HIGH-RESOLUTION MICROWAVE SPECTRA OF SOLAR BURSTS

M. STÄHLI*, D. E. GARY, and G. J. HURFORD

California Institute of Technology, Pasadena, CA 91125, U.S.A.

(Received 20 September, 1988; in revised form 5 December, 1988)

Abstract. Microwave observations with exceptionally high spectral resolution are described for a set of 49 solar flares observed between May and October 1981. Total power data were obtained at 40 frequencies between 1 and 18 GHz by the Owens Valley frequency-agile interferometer with 10 s time resolution. Statistical analysis of this sample of microwave bursts established the following significant characteristics of their microwave spectra: (i) Most ($\approx 80\%$) of the microwave events displayed complex spectra consisting of more than one component during some or all of their lifetime. Single spectral component bursts are rare. It is shown that the presence of more than one component can lead to significant errors when data with low spectral resolution are used to determine the low-side spectral index. (ii) The high-resolution data show that many bursts have a low-side spectral index that is larger than the maximum value of about 3 that might be expected from theory. Possible explanations include the effect of the underlying active region on the perceived burst spectrum and/or the necessity for more accurate calculations for bursts with low effective temperatures. (iii) the peak frequencies of the bursts are remarkably constant during their lifetimes. This is contrary to expectations based on simple models in which the source size and ambient field remain constant during the evolution of a burst.

1. Introduction

Microwave bursts during the impulsive phase of solar flares are generally believed to be generated by gyrosynchrotron emission from energetic electrons interacting with the magnetic fields of active regions. The microwave radiation carries information about the physical parameters characterizing the source such as its magnetic field strength as well as information on the energy spectrum of accelerated electrons. Microwave bursts are discussed in several recent reviews (e.g., Kundu and Vlahos, 1982; Dulk, 1985; Crannell *et al.*, 1988).

Observations of solar microwave bursts in the range 1 to 30 GHz have been carried out primarily with two different classes of instrumentation. With imaging instruments such as the VLA it is possible to make spatially resolved maps at a few discrete frequencies. Alternatively, fixed-frequency radiometers have been used for many years to provide light curves at specific frequencies. These instruments usually receive the radiation from the whole Sun, so that no spatial information is available. Spectral resolution is only available by combining the data from radiometers at different frequencies. Examples of this class of instrumentation include the Radio Solar Telescope Network RSTN (Air Weather Service, 1982) and the Bern Radio Observatory in Switzerland (Magun *et al.*, 1981). Several receivers are also used by observatories in Japan, such as Toyokawa (Torii *et al.*, 1979) and Nobeyama (Nakajima *et al.*, 1985).

* Swiss National Science Foundation Fellow from the University of Bern.

Solar Physics **120** (1989) 351–368.

It should be noted that both classes of instrumentation are characterized by a frequency resolution of $\Delta\nu/\nu \geq 50\%$ (see Figure 1). Formation of spectra by combining measurements from different observatories is also hampered by different instrumental characteristics, calibration procedures, and acquisition times. Consequently, with existing instruments, only a coarse estimation of the spectral shape can be made and spectral structures finer than a few GHz are usually not detectable.

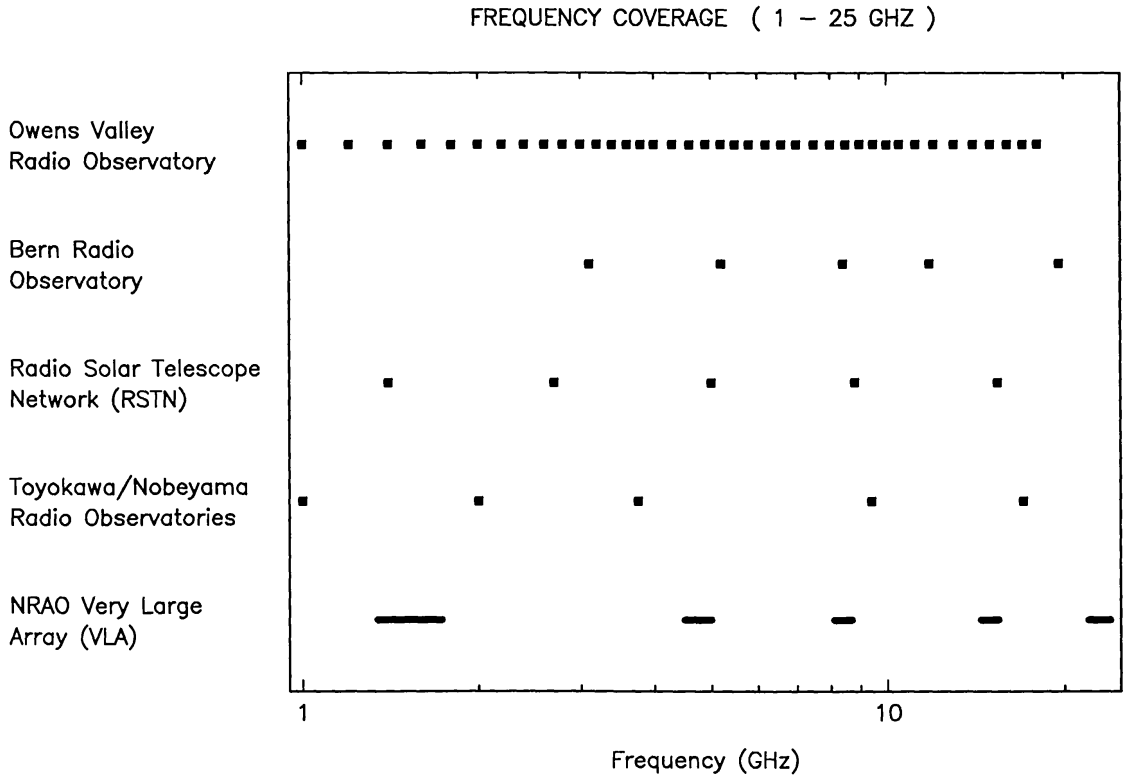

Fig. 1. A comparison of the frequency coverage of different observatories between 1 and 25 GHz. Some of the observatories mentioned have additional coverage at higher and lower frequencies. Bern observes at 3.1, 5.2, 8.4, 11.8, 19.6, 35.0, 50.0, and 92.5 GHz; RSTN at 0.245, 0.410, 0.606, 1.4, 2.7, 5.0, 8.8, 15.4, and 35.0 GHz; Toyokawa at 1.0, 2.0, 3.75, and 9.4 GHz and Nobeyama at 17.0, 35.0, and 80.0 GHz. The VLA uses six frequency bands, 0.3–0.35, 1.34–1.73, 4.5–5.0, 7.6–9.1, 14.4–15.4, and 22.0–24.0 GHz.

Probably the most complete investigation of microwave burst spectra to date was provided by Guidice and Castelli (1975). They performed a statistical analysis using data from the Sagamore Hill Radio Observatory with frequency coverage corresponding to RSTN. They classified the microwave bursts according to their spectral shapes at the maxima of the events. Because of the observational limitations mentioned above this classification gives only a rough picture of the microwave burst spectra.

Since 1981 much better frequency coverage in the range 1 to 18 GHz has been provided by the frequency-agile interferometer at the Owens Valley Radio Observatory. This instrument has obtained high spectral resolution data, first with a single antenna during 1981, and subsequently using two- and three-element interferometry. In this paper we present a phenomenological and statistical study of flares observed in total power with this instrument during several months of high solar activity in 1981. After

a presentation of the observations (Section 2) we will summarize briefly some relevant theoretical concepts in Section 3. The results of this investigation are presented and discussed in Section 4 and our conclusions summarized in Section 5.

2. Observations

During the previous solar maximum the fixed-frequency interferometer at the Owens Valley Radio Observatory (OVRO) was converted to a microwave spectrometer using frequency-agile receivers (Hurford, Read, and Zirin, 1984). In April 1981 the first of these receivers became operational. Mounted on one of the two 27 m antennas, it provided high spectral resolution data in total power while a fixed-frequency receiver on the other antenna observed with high time resolution (50 ms) at 10.6 GHz.

Between May and October 1981 extensive solar observations were carried out using the Owens Valley instrument in this 'hybrid' mode. The frequency-agile system measured the total power in both senses of the circular polarization at 40 frequencies in the range 1 to 18 GHz. Each frequency/polarization was sampled for 50 ms once every 10 s. As is shown in Figure 1, this frequency resolution represented a substantial improvement over what was previously available. The time resolution of 10 s proved adequate for the investigation of the overall behaviour of microwave bursts with typical durations in the order of minutes. Although different frequencies were sampled successively, during the data reduction light curves at each frequency were interpolated so that the spectra discussed below can be considered to have been effectively acquired simultaneously at all frequencies.

We carried out a systematic search through all the data collected during the 'hybrid' mode observations. If there were any indication of a burst, either from the HXRBS event listing (Dennis *et al.*, 1985), the SGD reports (solar radio emission outstanding occurrences) or as noted by the observer, we checked the corresponding time segment on our data tapes. We restricted ourselves to the events with an OVRO peak flux of more than 3 SFU. Some events were discarded because of saturation and/or tracking problems during the first month of observations.

Since at higher frequencies the field of view was restricted to less than the full Sun, special attention was given to the issue of antenna pointing. During the observations the instrument was usually pointed at the centroid of 10 GHz emission from an active region. Active region selection was usually based on a combination of Big Bear Solar Observatory's estimation of the region most likely to flare, and the Solar Maximum Mission observing plan. Some flares, of course, occurred elsewhere in the active region or in another active region altogether. This can be significant for the spectral analysis since the half-power beam width is frequency-dependent, varying inversely with the frequency from 2.6 arc min at 18 GHz to 46 arc min at 1 GHz. Therefore, the observed spectral shape of an off-axis event can be affected by pointing, particularly at the higher frequencies. Previous studies were not affected by this problem because most used instruments that viewed the whole Sun.

We used two methods to check the positions of the flares: (1) We compared the

coordinates of the beam center with the location of reported Hα flare and (2) we estimated the position of the source relative to the center of the primary beam by using squint modulation of the observed spectrum (Hurford, 1984). (Squint modulation provides a fine scale modulation of the observed spectrum which depends in a known manner on the displacement of the burst source location from the pointing axis of the telescope.) The first method can be inaccurate, since both reported flare positions and antenna pointing are subject to errors. The squint effect on the other hand can be used to correct the observed spectrum when the microwave burst has a peak flux density of more than about 10 to 15 SFU, a threshold necessary to ensure that the squint modulation is not dominated by noise. Only events which show a correct antenna pointing by at least one of these two methods were used for our analysis.

Our sample contains 29 events ($\approx 60\%$) which were corrected using squint modulation. Of the bursts in our sample with peak flux below the threshold for analysis using squint compensation, we included 20 for which the location of the associated Hα flare confirmed proper pointing of the antenna. Statistical comparison of these two classes of events showed no significant differences for the results reported here, except in terms of intensity, as might be expected from the threshold for the squint criteria. This study is based on these 49 events for which we have positive indication of correct antenna pointing (Table I).

The sample of 49 bursts provided a total of about 3000 individual spectra in total intensity (Stokes I). All data are fully calibrated using Cas A as a flux standard (Baars *et al.*, 1977) with a correction for the effect of its finite size. In the solar data, preflare signal levels have been subtracted at each frequency. Figure 2 shows examples of different types of burst spectra as seen in the OVRO data. The most common types are shown in Figure 2(a) and 2(d), as we discuss below. The temporal evolution of the spectrum of a typical, simple time profile event is given in Figure 3. Note that the peak frequency is nearly constant during more than a factor of 40 change in flux. The dashed arrows in the figure show the shift expected from theory, as discussed further in Section 4.4.

3. Theory

During a solar burst the radiation at frequencies >1 GHz is dominated by gyrosynchrotron emission, generated by energetic electrons with either a thermal or non-thermal energy distribution. At low effective temperatures, gyroresonance radiation or thermal bremsstrahlung may also be important, especially for small events, and under special conditions even plasma radiation is possible up to about 3 GHz. In the following, however, we will consider only the gyrosynchrotron emission. For a homogeneous source, i.e., a source with uniform magnetic field, electron density and temperature, the brightness temperature spectrum for gyrosynchrotron emission can be calculated. Over a wide range of parameters, its shape depends only on the electron energy distribution. However, in order to measure the brightness temperature spectrum of a burst it is necessary to image the source at all frequencies. Spectra reported to date, however, have

TABLE I

OVRO events 1981

Event number	Date	Time (UT)			Max. flux (SFU)	Peak freq. (GHz)
		Beg.	Max.	End		
1	30 June	17:46	17:50	>18:00	4	6.5
2	30 June	20:36	20:38	>20:45	7	5.0
3	1 July	22:51	22:52	22:54	35	6.8
4	6 July	18:58	19:20	>19:25	5	7.7
5	17 July	21:48	21:56	>22:20	10	8.3
6	17 July	23:17	23:20	23:25	11	8.5
7	18 July	16:31	16:34	16:50	11	8.0
8	18 July	17:37	17:38	17:40	77	8.3
9	18 July	19:32	19:33	19:34	4	7.8
10	21 July	18:11	18:13	>18:17	30	7.5
11	21 July	21:01	21:03	21:08	9	6.2
12	22 July	20:47	20:49	20:51	15	9.1
13	24 July	18:26	18:28	18:36	83	7.7
14	24 July	22:41	22:42	22:53	81	10.8
15	27 July	18:14	18:15	>18:20	17	7.3
16	27 July	21:37	21:38	21:44	12	7.8
17	27 July	22:09	22:12	22:19	12	5.5
18	28 July	16:40	16:41	16:46	41	7.1
19	28 July	18:34	18:36	18:41	23	9.4
20	31 July	19:39	19:41	19:43	4	3.2
21	3 Aug.	20:21	20:24	20:29	240	10.0
22	4 Aug.	23:26	23:27	23:37	17	9.0
23	6 Aug.	19:11	19:12	19:22	15	9.5
24	7 Aug.	18:57	19:07	>20:00	620	5.0
25	8 Aug.	17:11	17:13	>17:20	10	6.1
26	8 Aug.	22:24	22:33	22:44	5	9.5
27	10 Aug.	22:43	22:44	22:46	7	7.4
28	12 Aug.	19:42	19:44	20:00	13	10.0
29	12 Aug.	20:55	21:06	>21:35	95	10.0
30	13 Aug.	21:36	21:38	21:41	8	8.3
31	13 Aug.	23:09	23:15	>23:24	9	3.0
32	14 Aug.	18:22	18:25	>18:30	40	5.5
33	16 Aug.	19:30	19:38	>20:35	15	8.0
34	6 Sept.	16:24	16:27	>16:35	6	7.5
35	6 Sept.	18:10	18:13	18:17	26	8.4
36	6 Sept.	21:02	21:12	>21:23	23	7.7
37	7 Sept.	16:56	17:00	17:15	30	6.9
38	7 Sept.	18:05	18:21	>19:00	20	5.2
39	7 Sept.	20:54	20:55	21:01	11	7.0
40	8 Sept.	16:58	17:03	>17:40	74	7.2
41	8 Sept.	17:42	17:43	17:49	20	4.0
42	8 Sept.	19:00	19:02	19:05	20	7.1
43	13 Sept.	22:14	22:16	22:21	9	6.2
44	13 Sept.	22:25	22:27	>22:36	10	6.8
45	28 Sept.	19:17	19:17	19:21	15	5.3
46	3 Oct.	20:05	20:06	20:09	14	4.0
47	16 Oct.	18:49	18:51	18:53	20	6.6
48	16 Oct.	20:32	20:34	20:57	32	6.9
49	19 Oct.	23:06	23:27	>23:33	35	8.0

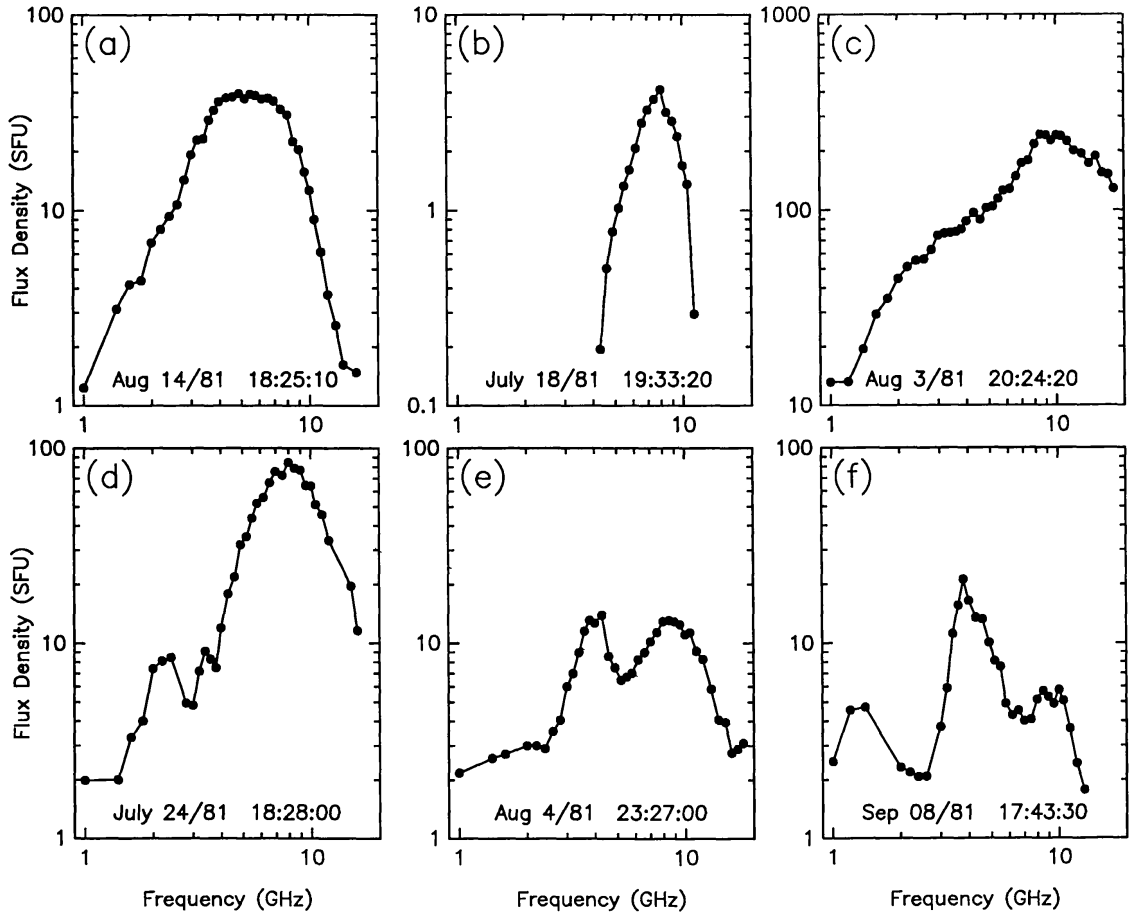

Fig. 2. Examples of high-resolution burst spectra. The flux density is plotted versus the frequency in a double logarithmic scale for one particular time. We found such different types of spectra as simple (a), narrow band (b), broad band (c), and complex (d), (e), (f).

been flux density spectra. To predict the flux density spectrum an additional assumption about the frequency dependence of the source size is necessary. Figure 4 gives the shape of expected spectra for a homogeneous source, whose size therefore is independent of frequency. These spectra were calculated by Gary and Hurford (1988) using the expressions for gyrosynchrotron emission given by Dulk and Marsh (1982). The shape of the curves is nearly independent of the parameters, whereas the location of the curves is different for different sets of parameters. Arrows in the figure represent the direction and magnitude of shift when the corresponding parameter increases by a factor of two.

It should be noted, however, that the shape of the curves is affected by source inhomogeneities. For example, a magnetic field gradient, which implies a decreasing source size with increasing frequency, or a electron temperature gradient would affect the spectral slopes (see Dulk and Dennis, 1982). The slope of the optically thick part of the spectrum (low-frequency slope) would become shallower resulting in a broader spectrum. Simultaneous emission from several sources with different parameters (multiple sources) may flatten the observed spectra (Klein, Trottet, and Magun, 1986), or appear as separate spectral components.

In order to compare theory with observations it is conventient to summarize the

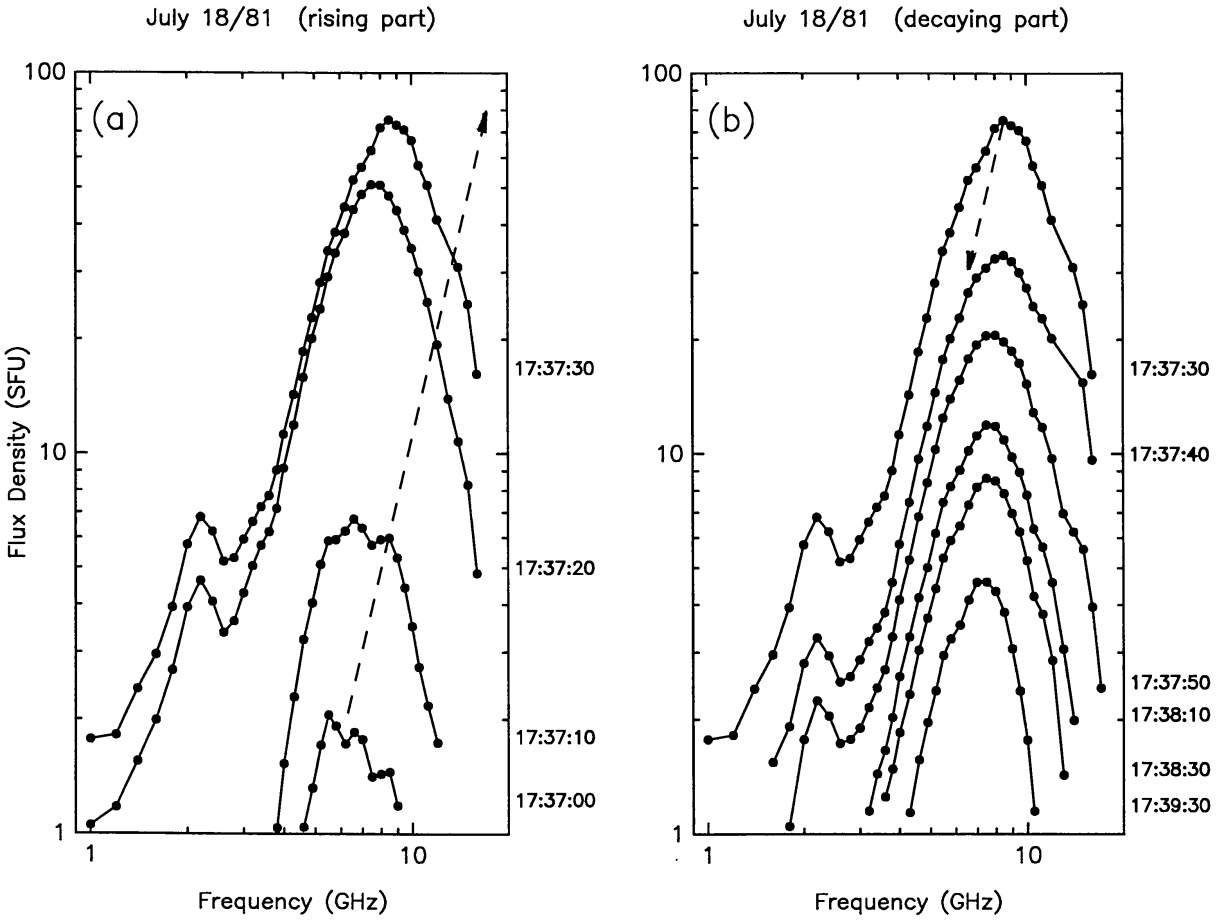

Fig. 3. Example of the temporal evolution of a microwave burst spectrum: The observed flux density is plotted versus the frequency for several times during the rising phase of the burst (a) and during the decay of the event (b). For this plot the data have been smoothed by performing a running mean over three consecutive frequencies. The dashed arrows indicate the minimum peak frequency shifts expected for gyrosynchrotron emission of a homogeneous source (for details see Section 4).

observed microwave spectra quantitatively. With reference to a double logarithmic plot of flux density versus frequency, a single component spectrum can be characterized by four parameters: peak frequency, peak flux, low-frequency slope, and high-frequency slope. The four parameters define the shape of the observed spectra, and from them we can estimate the source parameters and their temporal evolution throughout the microwave event. In order to determine the four parameters, we fit the observed spectra with the following function by using a least-squares technique:

$$S = A\nu^{a}(1 - e^{-B\nu^{-b}}) . \tag{1}$$

This equation is a general expression for the frequency (ν) dependence of the flux density S. The fitting parameters are A, B, a, and b. This expression is given by the radiative transfer equation reduced to the special case of an isolated source with constant effective temperature of the radiating electrons T_{eff} (e.g., Dulk and Marsh, 1982):

$$T_b = T_{\text{eff}}(1 - e^{-\tau_\nu}) . \tag{2}$$

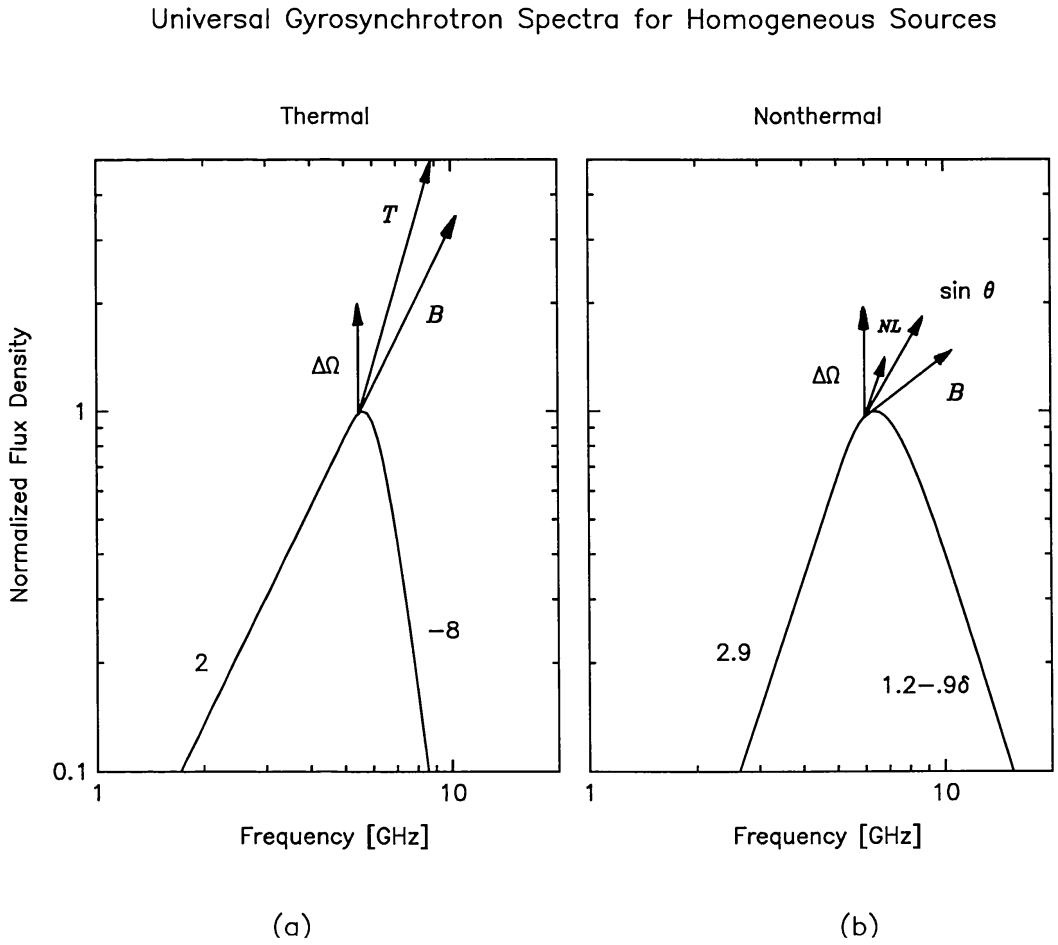

Fig. 4. Expected flux density spectra for thermal (a) and nonthermal (b) gyrosynchrotron emission of a homogeneous source. The arrows represent the direction and the magnitude of the shift of the spectrum when the corresponding parameter increases by a factor of two (from Gary and Hurford, 1988).

Equation (1) is suggested from Equation (2) and $S = \Delta\Omega k T_b \nu^2/c^2$, for emission mechanisms with T_{eff} and τ_ν proportional to a power of ν. These requirements are fulfilled by the simplified expressions for the gyrosynchrotron radiation from mildly relativistic, nonthermal and thermal electrons given by Dulk and Marsh (1982). Equation (1) is, therefore, applicable over the range of validity of these approximations.

Once the four parameters A, B, a, b of the fit function are known, the four basic characteristics, low-frequency slope (corresponds to a), high-frequency slope ($a - b$), peak flux and peak frequency can be calculated. The values found by this method are relatively immune to noise in the data. A complex spectrum with several components, however, can lead to incorrect fits. Some broad band spectra also cannot be fit very accurately. The simple theoretical shape given by Equation (1) has the property that the bandwidth is given by the slopes. Therefore, fits of observed spectra with a flat top tend to give a peak flux which is too high or slopes which are too shallow. (Such spectra might be due to inhomogeneous sources.) In such cases fit parameters were determined by hand.

As we will discuss in the following section, many of the spectra were not simple but

instead consisted of more than one spectral component. However, the fits could still be applied by limiting the frequency range used to that corresponding to the dominant spectral peak.

Spectral fits were carried out for all 3000 observed spectra. In the next section we will describe the characteristics of the observed spectra, drawing upon the results of this fitting procedure.

4. Results

4.1. The shape of microwave burst spectra

During an initial examination of the bursts, we noticed that many of the 49 microwave events had a complex spectrum, consisting of more than one spectral component. In particular, at the time of maximum flux density, we found that 32 events ($\approx 65\%$) show several spectral components. Furthermore, 8 of the remaining 17 events have complex spectra during some other part of their lifetime. Therefore, more than 80% of the microwave events have complex spectra consisting of more than one component. About 80% of the minor spectral components occur on the low-frequency side of the main peak in the spectrum, i.e., at frequencies lower than the peak frequency, as in Figure 2(d).

This result is in contrast to the results of Guidice and Castelli (1975). Classifying more than 2400 radio bursts observed by the Sagamore Hill Radio Observatory from 1968 to 1971 at 9 frequencies in the range from 0.245 to 35 GHz, they found that only about 5% of the events have complex microwave spectra. One reason for the discrepancy between the Sagamore Hill data and the OVRO data is the difference in frequency resolution. With a frequency resolution of $\Delta\nu/\nu \geq 50\%$ most of the spectral fine structures observed here could not have been resolved and so were missed in the low-resolution data. We conclude that bursts with multiple spectral components are far more common than has been previously supposed. We shall show below that this fact has important consequences for measuring the low-frequency slope from patrol data.

4.2. The 'typical' microwave burst

With the results from our fit analysis, it is of interest to calculate the parameters of the main spectral component of a 'typical' microwave burst. We averaged our data for three different phases of a burst: rise, maximum and decay. Rise and decay were chosen to be at the times when the flux density is a factor of e lower than at the maximum of the event. We have disregarded parameters whose accuracy is questionable due to excessive scatter in the data or in cases where there were not enough data points for the determination of the slopes.

Table II contains the averages of the basic spectral parameters for the three different times along with the corresponding standard errors in the mean. The values do not change significantly from rise to maximum and decay of the burst with the exception of a slight increase of the bandwidth throughout the event. The distribution of the maximum flux density of our events is illustrated by the histogram in Figure 5. Very

TABLE II

The typical microwave burst

Parameter	Rise	Maximum	Decay
LF slope	3.4 ± 0.3	3.1 ± 0.2	3.0 ± 0.3
HF slope	−3.6 ± 0.3	−3.7 ± 0.2	−3.7 ± 0.3
Peak frequency (GHz)	7.5 ± 0.3	7.2 ± 0.3	7.4 ± 0.3
FWHM bandwidth (%)	80 ± 5	85 ± 5	95 ± 5

intense events are rare in our sample as a result of saturation. Most of the events have a duration on the order of minutes. The distribution of the peak frequencies is shown in Figure 6. Although it is possible that the peak frequency of some events is higher than 18 GHz and that we observed only a subsidiary spectral component, this possibility is not very likely, in view of the relative absence of peaks between 11 and 18 GHz, and the fact that none of the events had microwave emission reported in the SGD data at frequencies greater than 17 GHz.

As already mentioned in Section 3, the bandwidth of the theoretical curve (Equation (1)) is given by the slopes. It is $\approx 70\%$ for rise, maximum and decay, if the slopes from Table II are used for the calculation. The fact that the observed bandwidths

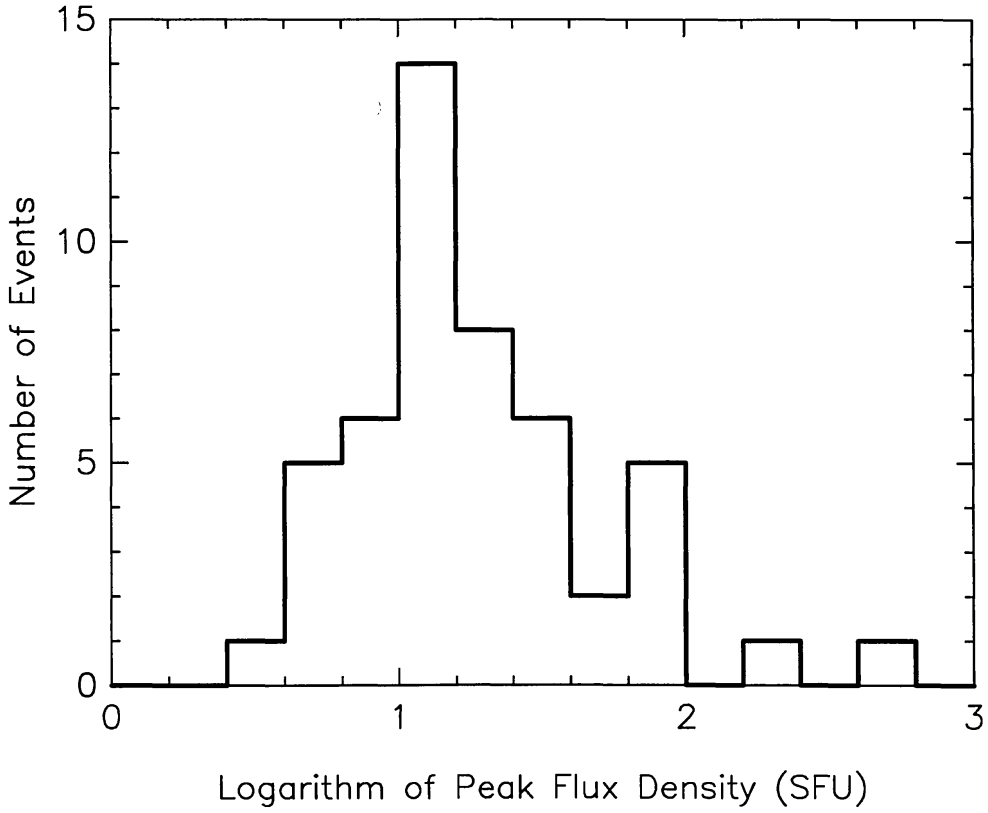

Fig. 5. Histogram of maximum flux density (logarithmic) for all the events in our sample. The cutoff at 3 s.f.u. is due to event selection criteria discussed in the text.

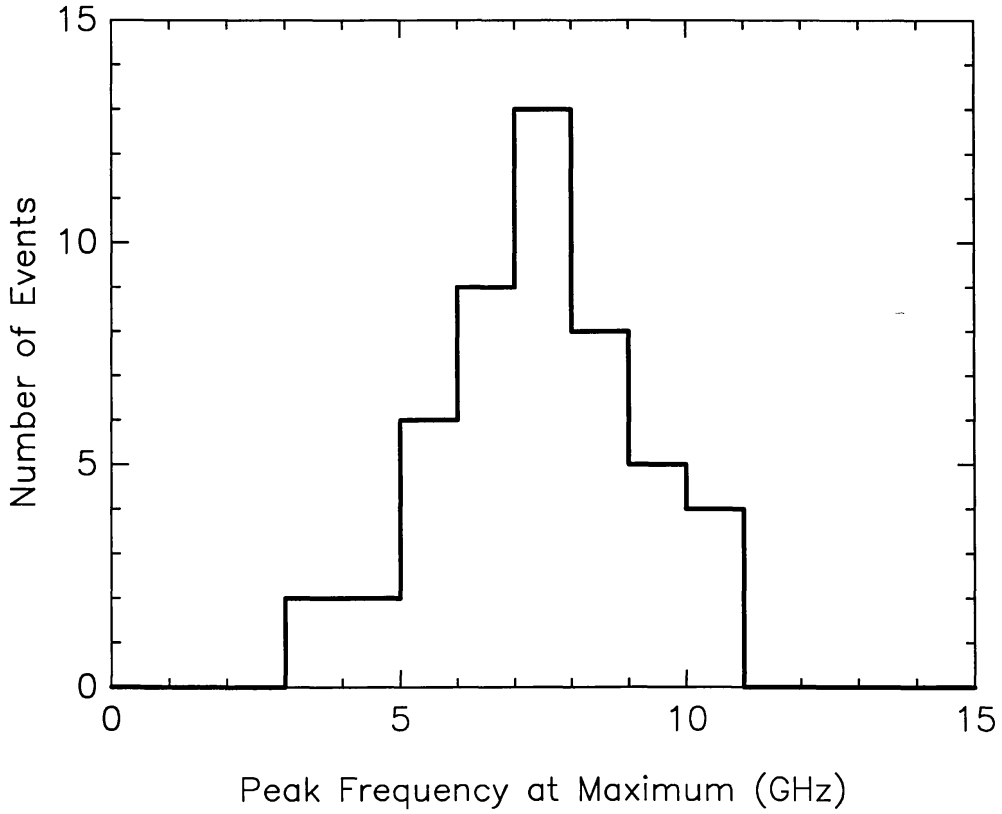

Fig. 6. Histogram showing the distribution of the peak frequencies at the maximum of the events.

are larger (80–95%) indicates that most of the events have a spectrum that is somewhat broader than that expected from theory for a homogeneous source.

4.3. The low-frequency slope

An interesting result was found for the low-frequency slope. The histograms (Figure 7) show that many bursts have a spectral index which is greater than 3. In fact, slopes up to 10 have been observed. This is remarkable since the simplified theory for homogeneous sources (see Figure 4) would suggest slopes of 2 or 3 and the effect of inhomogeneities is to decrease the low-frequency slope. During the rising part 48% of the events are found to have an index > 3. At the maximum 40% and during the decay phase 44% of the events have a low-frequency slope > 3. An example of a burst with such a steep spectrum is shown in Figure 8 together with the slopes expected from theory for a homogeneous source (about 2 for thermal and about 3 for nonthermal gyrosynchrotron radiation).

Why were such steep spectra not previously observed? To investigate this, we repeated our analysis of the 49 events using only five frequencies (1.4, 2.8, 5.2, 8.5, and 15.0 GHz) which approximately correspond to the RSTN frequencies. A comparison of the low-frequency slopes from the two different fits is given in Table III, which shows for example that only 6% of the low-resolution fits would have appeared too steep, compared to 40% for the high-resolution data. The reason for this discrepancy is related to the fact that the minor spectral components, which mainly appear at frequencies

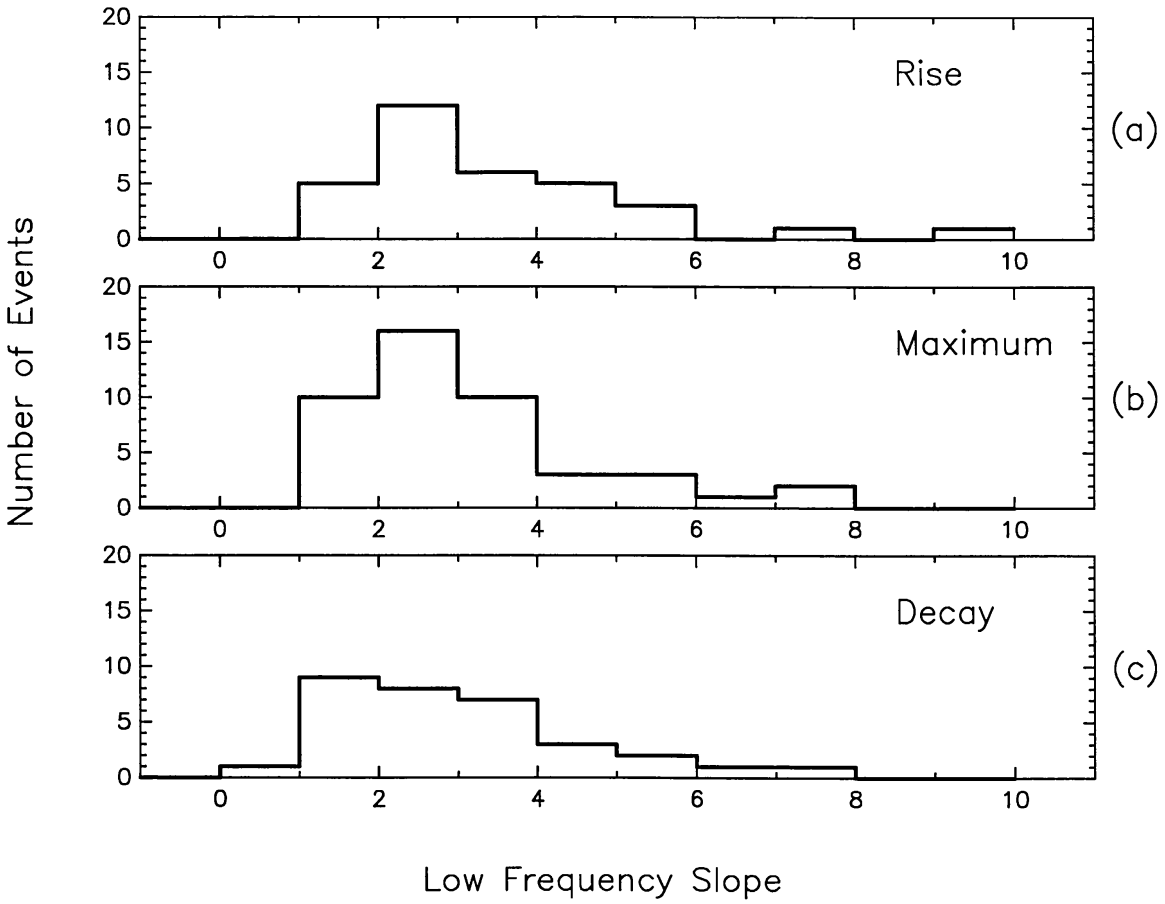

Fig. 7. Histograms for the low frequency slopes of the events at the rise (a), the maximum (b), and the decay (c) of the events. Note that many events show slopes > 3.

smaller than the peak frequency, are not resolved by the low spectral resolution data and instead cause the low-frequency slope to appear flatter. Figure 9 shows an example for which the analysis with the reduced set of 5 frequencies gives a value for the low-frequency slope of 2.1, whereas the slope of the dominant spectral component is actually 3.5.

How can such steep spectra be explained? One approach is to invoke an absorption mechanism that mainly affects the radiation at lower frequencies. Different absorption processes have been discussed in the literature (e.g., Melrose, 1980), such as

TABLE III

The low side spectral index

	Average LF slope		Fraction of events with LF slope > 3	
	5 freq.	40 freq.	5 freq.	40 freq.
Rise	2.1 ± 0.2	3.4 ± 0.3	17%	48%
Maximum	1.9 ± 0.1	3.1 ± 0.2	6%	40%
Decay	1.7 ± 0.1	3.0 ± 0.3	3%	44%

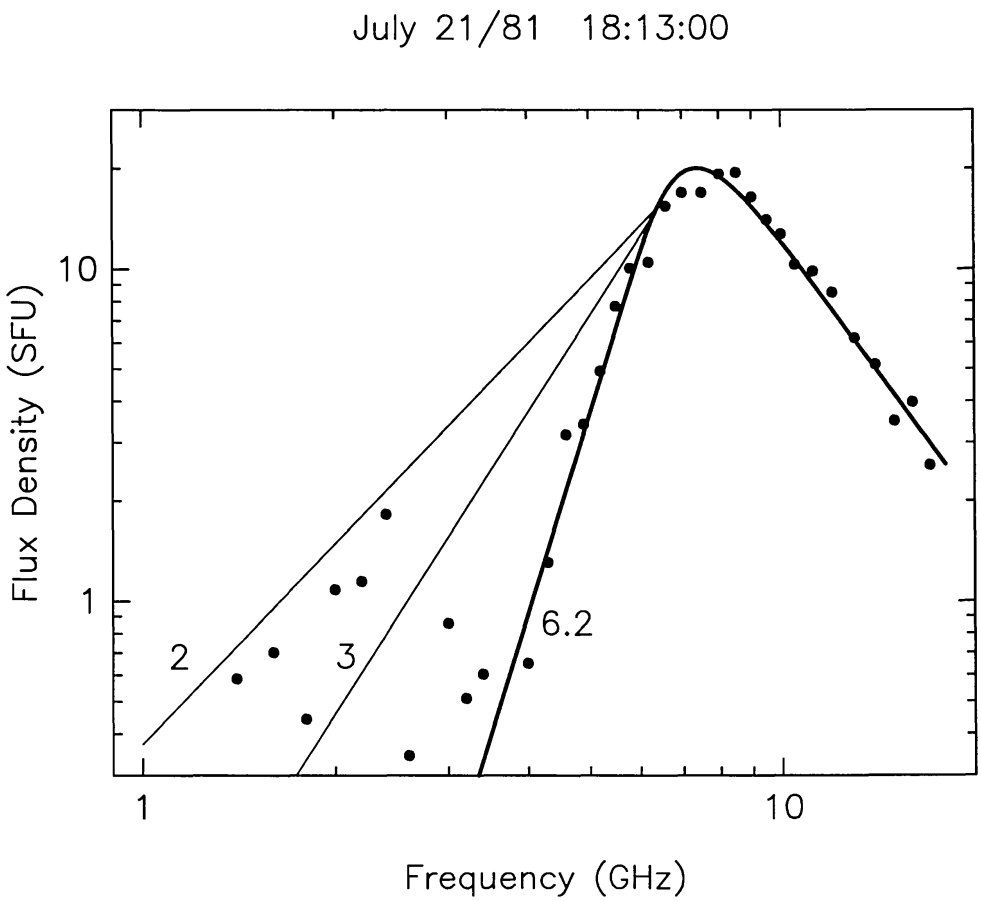

Fig. 8. Example of a spectrum with a steep low-frequency slope. The observed data points and the fit are shown together with the slopes expected from theory for a homogeneous source (about 2 for thermal and about 3 for nonthermal gyrosynchrotron emission). The low frequency slope found by the fit is 6.2.

Razin–Tsytovich suppression, free-free absorption, and gyroresonance absorption. Razin suppression occurs in a dense plasma for frequencies

$$\nu \leq \nu_p^2/\nu_B\,, \tag{3}$$

where ν_p and ν_B stand for the plasma frequency and the gyrofrequency, respectively. In order to explain the majority of the observed steep spectra the absorption process has to be effective at least up to ≈ 5 GHz. The required electron density n_e (in cm^{-3}) then is

$$n_e \geq 1.7 \times 10^8 B \tag{4}$$

for a given magnetic field strength B (in G). Assuming the lowest acceptable magnetic field of 100 G the minimum electron density for Razin suppression, therefore, is $\approx 2 \times 10^{10}\ \mathrm{cm}^{-3}$, which is rather high. Higher B requires even higher densities. Free-free absorption also requires a high density, low temperature ambient plasma, whereas the gyroresonance absorption requires a strong magnetic field along the line-of-sight, outside the flaring region. Any or all of these absorption mechanisms can be important in some bursts with special source geometries as in limb flares (Dulk, Bastian, and Kane, 1986). However, it is not likely that such special conditions occur for the majority of

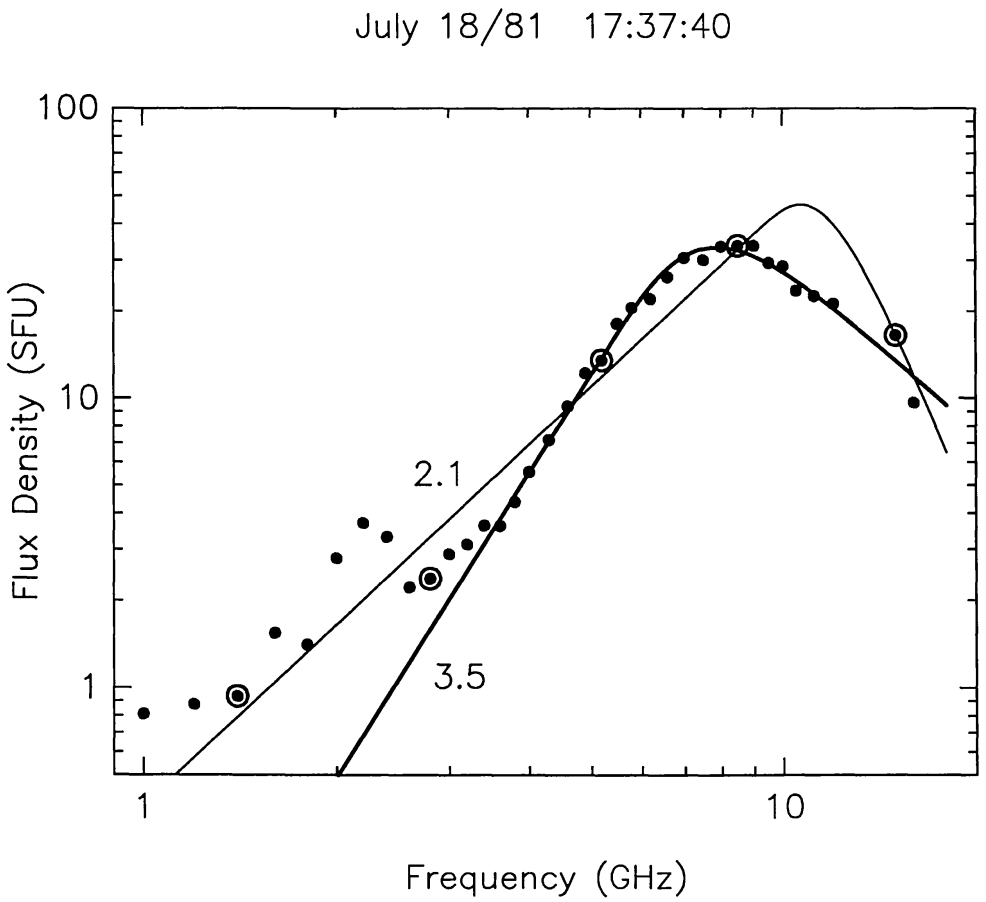

Fig. 9. Example of a spectrum in which the spectral coverage affects the fitted spectral parameters. The spectrum is fit by the function $S = A\nu^{a}(1 - e^{-B\nu^{-b}})$ using only the five circled frequencies corresponding to the RSTN frequencies (thin line) and all 40 frequencies (thick line). The low frequency slopes found by these fits are 2.1 and 3.5, respectively.

the microwave events. In the following we will discuss two other mechanisms which can be important under more common circumstances.

Microwave bursts nearly always occur above active regions on the Sun. These active regions emit microwave radiation with a brightness temperature T_b of up to 5×10^6 K due to free-free and gyroresonance emission. In order to separate the flux densities of the burst and the underlying active region, conventional practice is to subtract the preflare level at each frequency. However, in the presence of an underlying active region, this procedure induces an error in the optically thick part of the flare spectrum. At these frequencies the radiation from that part of the underlying active region that is masked by the optically thick flare radiation no longer contributes to the measured flux density and, therefore, should not be subtracted. Preflare subtraction then results in a flux density that is too small at low frequencies, so that the perceived flare spectrum appears to be steeper than it should be. At any given frequency the magnitude of the error depends on the relative brightness temperature of the flare and underlying active region, and on the optical depth and area of the flare emission. The effect is independent of the active region optical depth, except insofar as it affects the active region brightness temperature.

For typical burst sizes and active region temperatures, the maximum error at low frequencies corresponds to a few solar flux units. Though this error affects all bursts occurring above an active region, the spectral shape of small events is particularly affected whereas more intense events with a much higher brightness temperature than the underlying region are relatively immune. Precise correction for such effect would require knowledge of the brightness temperature T_b of the underlying active region and the flare as a function of both frequency and position.

Another possible explanation for steep spectra on the low-frequency side are 'low effective temperature bursts'. For weak events with brightness temperatures $T_b \leq 10^7$ K low harmonics $\nu/\nu_B < 10$ are important. In this case the approximations of Dulk and Marsh (1982) are no longer valid and the exact expressions for gyrosynchrotron emission (Ramaty, 1969) must be used. We found that in this range of the parameters the optically thick part of the gyrosynchrotron spectrum is significantly steeper than for bursts with higher effective temperatures and a low-frequency slope greater than 3 is possible.

Both of these mechanisms, 'underlying active region' and 'low effective temperature bursts', can explain steep spectra for small events. The scatterplot (Figure 10) shows the distribution of the observed low-frequency slope against the flux density. This plot contains the data points for the rise, maximum and decay of all the bursts. There is some suggestion that small events tend to have steeper spectra as there are no spectra with

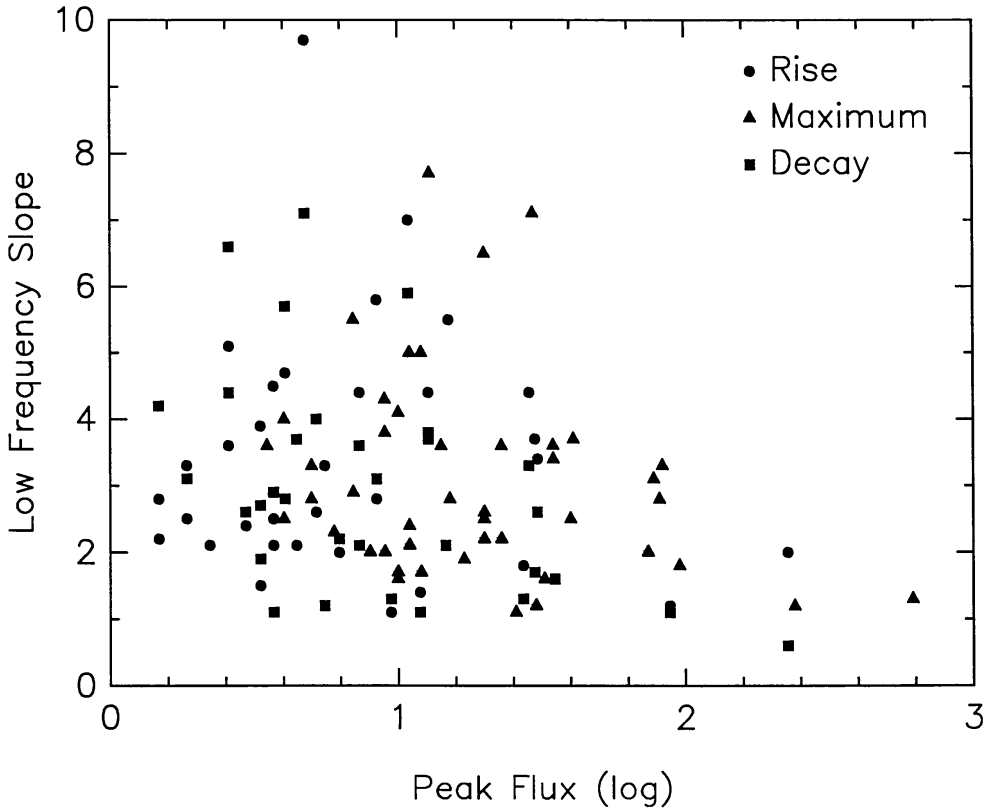

Fig. 10. Scatterplot of the low-frequency slopes as a function of the peak flux densities. There are three data points for each event corresponding to the spectrum at rise, maximum and decay of the bursts.

a peak flux of more than 90 SFU which are steeper than 3 on the low-frequency side. Furthermore, there is a trend for steeper spectra during rise and decay (48% and 44% with low-frequency slope > 3) compared to the spectrum at the maximum of the event (40% with low-frequency slope > 3). Additional evidence for a flux-related explanation for the slopes is the fact that none of the events in our sample deviates from a spectrum with slope 3 or less by more than 4 SFU. This relationship between peak flux and low-frequency slope perhaps makes it more likely that either the 'underlying active region' and/or the 'low effective temperature' mechanism is the explanation as distinct from one of the absorption processes, which would be expected to affect the spectra independently of the flux density.

4.4. The peak frequency

Another significant result of the statistical analysis is the temporal behaviour of the peak frequency. We have found that it stays remarkably constant throughout a burst, as in the example shown in Figure 3. For a constant source size $\Delta\Omega$ and a constant magnetic field strength B, theory predicts an increase of the peak frequency during the rising part of the burst, i.e., the phase from the beginning to the maximum of the event. The amount of the peak frequency shift is indicated in Figure 4 by the T arrow in the case of thermal gyrosynchrotron emission and by the NL arrow in the nonthermal case (for constant θ). The smallest peak frequency shift is expected in the thermal case because the T arrow has a steeper slope than the NL arrow. Therefore, the frequency increase is at least about 32% for a flux density increase by a factor of e. The dashed arrows in Figure 3 show the expected shift in peak frequency compared with a typical burst. Figure 11(a) summarizes the observed frequency shifts during the rise for all the bursts for which it could be measured together with the predicted minimum frequency shifts. The expected shifts were calculated using the observed peak frequency distribution. This figure shows that whereas the theory predicts an average shift of more than 2 GHz, the observations nearly do not show any shift on the average. A corresponding discrepancy between observations and theory exists for the decaying phase of the events (Figure 11(b)). In our sample of 49 bursts, only 2 events ($\approx 4\%$) display a frequency shift comparable to that expected from theory. We do not have an explanation for this remarkable constancy of the peak frequency.

5. Conclusions

This phenomenological study of high-resolution microwave burst spectra between 1 and 18 GHz showed that most of the events ($\approx 80\%$) have a complex spectrum consisting of more than one spectral component. This implies that the microwave radiation of a burst usually does not come from a single homogeneous source. It would suggest that the radiation originates at several individual sources with different source parameters. This result is supported by VLA observations at multiple frequencies (see, e.g., Shevgaonkar and Kundu, 1985; Dulk, Bastian, and Kane, 1986) which show distinct morphologies and/or locations at pairs of frequencies separated by an octave or more.

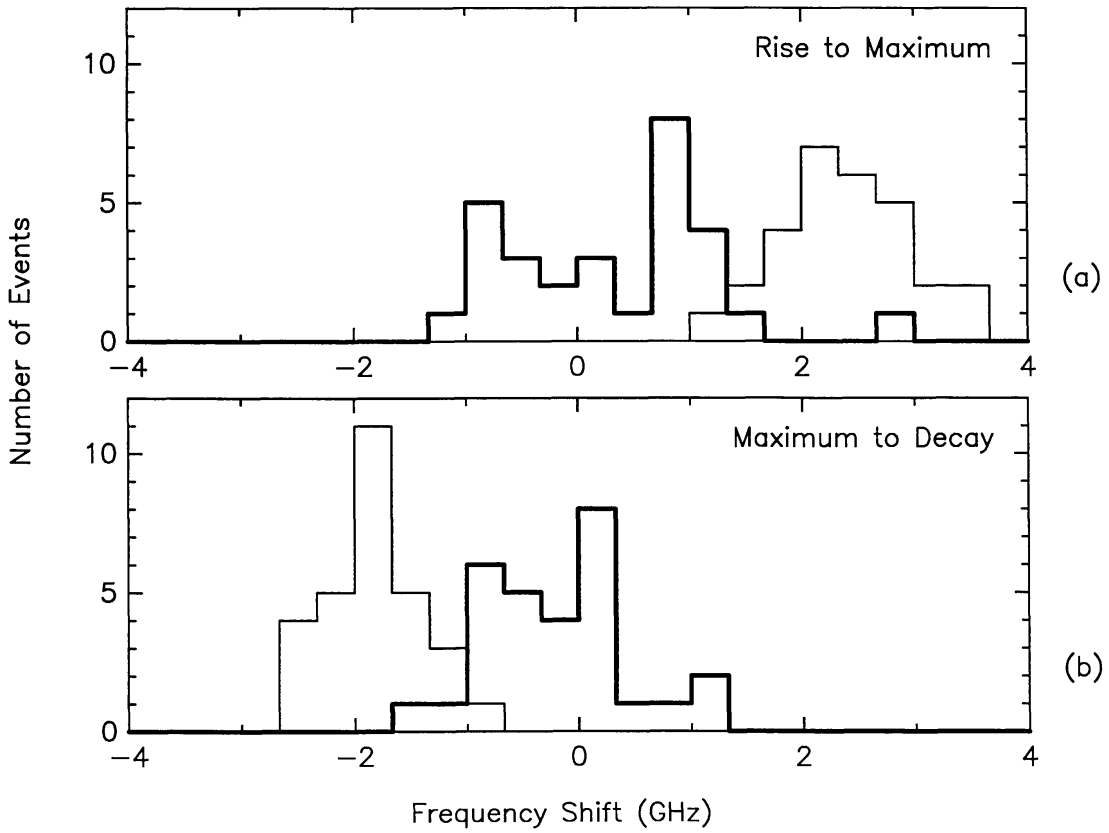

Fig. 11. Histograms of the measured peak frequency shifts (thick line) and the expected frequency shifts (thin line) for the rising phase of the burst (a) and the decaying part (b) of the events. The theoretical values give the minimum shift expected for constant source size and magnetic field. They were calculated by using the observed peak frequency distribution.

The low-frequency slope of a single spectral component was found to be often steeper than might be expected. Although in particular cases the steep spectra could be explained by absorption processes, a more likely explanation for the majority of events involves either the effect of an underlying active region and/or the necessity of using the exact theory for low effective temperature bursts. The very presence of steep low-frequency slopes, however, strongly suggests that the individual elementary microwave source corresponding to a single spectral component is relatively homogeneous since significant inhomogeneities would have tended to moderate the steep spectra.

We also found that the peak frequency stays nearly constant throughout a microwave event. This is in contrast to the theory which predicts a large variation of the peak frequency for a homogeneous source. Taken on its own, this result might suggest that for most of the events the source size and/or the magnetic field strength varies during the evolution of an event. At this point, however, the explanation for this spectral stability remains an open issue.

The low- and the high-frequency slopes of a microwave burst spectrum would give the best indication for the exact emission mechanisms and especially for the nature of the radiating electrons (thermal or nonthermal). Such source geometries as multiple sources and inhomogeneities, however, can strongly affect these slopes. Therefore,

spatially resolved observations of the microwave spectrum are needed in order to resolve the source inhomogeneities. Such observations would provide much more information about the emission mechanism and the source parameters of microwave bursts. With the resurgence in solar activity, spatially resolved spectral observations to achieve this are being acquired with the Owens Valley interferometer and will be discussed in subsequent papers.

Acknowledgements

We gratefully acknowledge the helpful discussions with Dr H. Zirin. The work was supported by NSF grants ATM-8610330 and AST-8702682 and by NASA NAG 5–946 to the California Institute of Technology. This study was carried out while one of the authors (MS) was a visiting scientist at the California Institute of Technology with a fellowship from the Swiss National Science Foundation.

References

Air Weather Service Pamphlet 105–61, 1 April 1982, Scott AFB, Il., U.S.A.
Baars, J. W. M., Genzel, R., Pauliny-Toth, I. I. K., and Witzel, A.: 1977, *Astron. Astrophys.* **61**, 99.
Crannell, C. J., Dulk, G. A., Kosugi, T., and Magun, A.: 1988, *Solar Phys.* **118**, 155.
Dennis, B. R., Orwig, L. E., Kiplinger, A. L., Gibson, B. R., Kennard, G. S., and Tolbert, A. K.: 1985, *NASA Technical Memorandum* 86236.
Dulk, G. A.: 1985, *Ann. Rev. Astron. Astrophys.* **23**, 169.
Dulk, G. A. and Dennis, B. R.: 1982, *Astrophys. J.* **260**, 875.
Dulk, G. A. and Marsh, K. A.: 1982, *Astrophys. J.* **259**, 350.
Dulk, G. A., Bastian, T. S., and Kane, S. R.: 1986, *Astrophys. J.* **300**, 438.
Gary, D. E. and Hurford, G. J.: 1988, *AGU Monograph Series* (in press).
Guidice, D. A. and Castelli, J. P.: 1975, *Solar Phys.* **44**, 155.
Hurford, G. J.: 1984, in *INDO-US Workshop 1984, Solar Terrestrial Physics*, National Physical Laboratory, New Delhi, p. 259.
Hurford, G. J., Read, R. B., and Zirin, H.: 1984, *Solar Phys.* **94**, 413.
Klein, K.-L., Trottet, G., and Magun, A.: 1986, *Solar Phys.* **104**, 243.
Kundu, M. R. and Vlahos, L.: 1982, *Space Sci. Rev.* **32**, 405.
Magun, A., Fuhrer, M., Kämpfer, N., Schöchlin, W., Stähli, M., and Wülser, J. P.: 1981, *Bern Solar Obs. Report* **46**.
Melrose, D. B.: 1980, *Plasma Astrophysics*, Vol. 2, Gordon & Breach, New York.
Nakajima, H., Sekiguchi, H., Sawa, M., Kai, K., Kawashima, S., Kosugi, T., Shibuya, N., Shinohara, N., and Shiomi, Y.: 1985, *Publ. Astron. Soc. Japan* **37**, 163.
Ramaty, R.: 1969, *Astrophys. J.* **158**, 753.
Shevgaonkar, R. K. and Kundu, M. R.: 1985, *Astrophys. J.* **292**, 733.
Torii, C., Tsukiji, Y., Kobayashi, S., Yoshimi, N., Tanaka, H., and Enome, S.: 1979, *Proc. Res. Inst. Atmospherics, Nagoya Univ.* **26**, 129.